Direct Z-scheme GdFeO3/g-C3N4 heterostructures with outstanding photocatalytic activity

Li Li
Huainan Normal University
Fengwu Wang (fwwang@126.com)
Huainan Normal University https://orcid.org/0000-0003-3627-1067
Jiajun Feng
Huainan Normal University
Siqi Guo
Huainan Normal University
Mai Xu
Huainan Normal University
Longde Wang
Huainan Normal University
Guiying Quan
Huainan Normal University

Research Article

Keywords: GdFeO3/g-C3N4, photocatalysis, visible light, Z-scheme

Posted Date: March 2nd, 2021

DOI: https://doi.org/10.21203/rs.3.rs-255210/v1

Abstract

The direct Z-scheme $GdFeO_3$/g-C_3N_4 photocatalysts used without any mediators were obtained using an ultrasonic synthesis approach. The composites' structures, elemental composition and morphologies, as well as optical, electrochemical and catalytic properties, were thoroughly analyzed. $GdFeO_3$/g-C_3N_4-3:7 composite exhibited an excellent enhanced light-harvesting ability and low recombination rate, which manifested into an outstanding visible-light driven activity, 7.7 and 2.3 times more than of stand-alone g-C_3N_4 and $GdFeO_3$, respectively. A mechanism responsible for the photocatalytic property enhancement was proposed. The stability and reusability of the $GdFeO_3$/g-C_3N_4 composites make them excellent materials for practical applications related to the removal of organic pollutants from the wastewater.

1. Introduction

Environment deterioration, including water contamination, is becoming more and more alarming as the energy consumed by the population and its industrial activities increase[1,2]. The photocatalytic assistance of nano-semiconductors attracts a lot of interest in pollutant degradation and removal from water and hydrogen energy production because of their efficiency, cost-effectiveness, and environmental friendliness[3,4]. However, the development of the most common nano-photocatalysts (such as TiO_2, CdS, and WO_3) is hindered by their photo-corrosion, low sensitivity to the visible light, and rapid recombination of photogenerated electron-hole pairs[5,6]. Many research and development efforts are currently undertaken to improve these materials by doping, creating heterojunctions, and surface modification[7-9].

Perovskite-type ferrite oxides, such as $LnFeO_3$ (Ln = La, Sm, Y, Dy, Gd, Nd, etc.), are widely used as isolators, gas sensors, and optical switches as well as for enhancing magnetic materials and lithium-ion batteries because of their low density, excellent stability, low toxicity, inertness, and ease of production[10,11]. They also possess bandgaps (in the 1.9-2.5 eV range) suitable for visible-light-driven photocatalysis. Among these compounds is a $GdFeO_3$ (GFO) perovskite, which contains Gd^{3+} with a half-full 4*f* subshell and possesses stable structure, narrow bandgap, and excellent optical absorption and photocatalytic properties[12-14].

Carbon nitride (g-C_3N_4) with a layered graphite-like structure is a π-conjugated semiconductor with a narrow bandgap (equal to ~2.7 eV) and excellent photoactivity under visible light irradiation[15]. Its activity and quantum efficiency can be enhanced even more by doping and combining with other compounds. In fact, g-C_3N_4/Ag_2CrO_4, g-C_3N_4/BiOBr, BiOCl/g-C_3N_4, g-C_3N_4/$BiFeO_3$, $CeVO_4$/g-C_3N_4, TiO_2/g-C_3N_4, and $YFeO_3$/g-C_3N_4 heterostructures were successfully fabricated [16-22].

This paper reports the fabrication of novel magnetic $GdFeO_3$/g-C_3N_4 heterostructures, which, to the best of our knowledge, were fabricated and used for dye degradation reaction for the first time. We used a simple ultrasonic synthesis method to obtain heterostructures with a range of $GdFeO_3$:g-C_3N_4 ratios. The

heterogeneous visible-light catalytic activity of these heterostructures was tested using Rhodamine B (RhB). We also characterized the ability of these heterostructures to scavenge reactive species as well as their stability and reusability.

2. Experimental Section

2.1 $GdFeO_3$/g-C_3N_4 synthesis

All initial chemicals were analytically pure and used as received. $GdFeO_3$ perovskite oxide power has been synthesized by the glycol-assisted sol-gel rapid calcination process in the orthorhombic phase with the pbnm space group as reported by our research group[23]. 15 mmol of $Gd(NO_3)_3 \cdot 6H_2O$ and 15 mmol of $Fe(NO_3)_3 \cdot 9H_2O$ were stirred with 40 mL of ethylene glycol for 4 h at 80 °C, after which the sol was dried for 8 hours at 120 °C. The resultant material was calcined at 800 °C for 4 h, after which it was rinsed and dried. The resulting product was brown $GdFeO_3$ nano-powder. g-C_3N_4 nanosheets were synthesized using 5 g of melamine heated at 520 °C for 4 h in a muffle furnace. The product was washed for several times with distilled water and absolute ethanol and then at 80 °C for 10 h[24].

To synthesize $GdFeO_3$/g-C_3N_4 composites, 100 mg of $GdFeO_3$ and 900 mg of g-C_3N_4 NSs were ultrasonicated in ethanol at room temperature for 2.5 hours and then stirred overnight. The solid product (which was named GFO/CN-1:9, where 1:9 corresponds to the $GdFeO_3$:g-C_3N_4 weight ratio) was collected and dried for 4 hours at 80 °C. By adjusting the initial $GdFeO_3$:g-C_3N_4 weight ratio, we also synthesized GFO/CN-3:7, GFO/CN-1:1, GFO/CN-7:3, and GFO/CN-9:1 composites.

2.2 Characterization

Crystallinity and structures of the samples were characterized by the X-ray diffraction (XRD) conducted using Bruker-AXS D8 instrument operated with Cu K_α-radiation at 40 kV and 40 mA. The spectra were collected in the 20–80 2θ range. GFO/CN-3:7 sample was also characterized by a transmission electron Hitachi Model H-800 microscope (TEM) operated at 200 kV. X-ray photoelectron spectroscopy (XPS) was conducted by a Perkin-Elmer PHI-1600 ESCA instrument using an Mg Ka radiation as an X-ray source and a C 1s peak energy (equal to 284.6 eV) for calibration. The Purkinje General T1901 UV–Vis spectrophotometer (containing an integrating sphere attachment and $BaSO_4$ reflectance standard) was used to collect adsorption spectra. The photoluminescence (PL) data were obtained by the fluorescence F4600 spectrometer manufactured by Hitachi (Japan) using a 300 nm excitation wavelength. The electrochemical impedance spectra (EIS) were collected by a CHI660E workstation using a three-electrode system and 0.5 M KCl electrolyte.

2.3 Photocatalytic tests

The catalytic activities of our materials were evaluated at 25 ºC using rhodamine B (RhB) degradation reaction by a Zhengqiao ZQ-GHX-V apparatus. 500 W Xe lamp with an optical cutoff filter below 420 nm

was used for sample irradiation. For this purpose, 10 mg of a sample was mixed with the 10 mL of aqueous RhB solution and stirred in the dark for 1 h. Then, the reaction vessel was exposed to the visible light. Aliquots were taken out and centrifuged. The supernatant was then subjected to the UV-Vis spectrophotometry (performed using T1901 instrument manufactured by Purkinje General) to determine the amount of RhB (which was performed at its characteristic wavelength of 553 nm). The RhB degradation efficiency C/C_0 was calculated using initial (C_0) and time-dependent (C) RhB concentrations. The UV–vis diffuse reflectance spectroscopy (DRS) was used to assess light absorption.

3. Results And Discussion

XRD spectra of $GdFeO_3$ showed the most prominent peaks at 22.96°, 25.76°, 31.87°, 32.84°, 33.47°and 59.45°, which correspond to the (110), (111), (020), (112), (200) and (312) planes of orthorhombic $GdFeO_3$ according to the JCPDS card number 47-0067 (see Fig. 1, bottom curve). XRD spectrum of g-C_3N_4 showed a (002) peak at 27.5° according to the JCPDS card No. 87-1526 (see a black top curve in Fig. 1). XRD spectra of various $GdFeO_3$/g-C_3N_4 composites showed only $GdFeO_3$ and g-C_3N_4 peaks. The intensity of the g-C_3N_4 peaks increased as its content in the $GdFeO_3$/g-C_3N_4 composite increased.

TEM of the GFO/CN-3:7 showed $GdFeO_3$ nanoparticles uniformly distributed on the g-C_3N_4 nanosheets (see Fig. 2(a) and (b)). HRTEM revealed lattice fringes 0.273 nm apart (which correspond to the (112) plane of orthorhombic $GdFeO_3$) and very distinct g-C_3N_4/$GdFeO_3$ interface (see Fig. 2(c)). Thus, g-C_3N_4 nanosheets served as substrates for $GdFeO_3$ nanoparticle growth and also prevented their agglomeration and growth into larger particles. The presence of numerous nanoparticles is beneficial for a catalyst because they provide a large surface area. Additionally, a tight g-C_3N_4/$GdFeO_3$ interface is advantageous for the fast and efficient charge transfers [25].

XPS of the GFO/CN-3:7 sample showed two peaks centered at 710.6 and 724.4 eV, ascribed to Fe $2p_{3/2}$ and Fe $2p_{1/2}$, respectively (see Fig 3a). Thus, Fe(III) was in its oxide coordination[26]. Gd core level spectrum showed 4d peaks located at 141.6 and 147.3 eV (see Fig. 3b). The main feature of the Gd 4d photoemission arose from multiplet splitting of the 4d hole with $4f_7$ valence electrons, forming $_9D$ and $_7D$ final ionic states[27,28]. The main O form is O^{2-}, as indicated by the O 1s spectrum, consisting of two peaks at 529.2 and 531.3 eV (see Fig. 3c). These peaks correspond to the hydroxyl species (O_H) and the $GdFeO_3$ crystal lattice oxygen (O_L, both in Gd-O and Fe-O configurations)[29]. The broad and asymmetric N 1s peak was deconvoluted into peaks positioned at 399.64, 399.03, and 398.14 eV (see Fig. 3d), which were interpreted as belonging to the H–N–$(C)_2$ and N–$(C)_3$ as well as to C–N=C bonds of g-C_3N_4[30,31], respectively. The N 1s peak observed for the $GdFeO_3$/g-C_3N_4 was slightly shifted relative to the g-C_3N_4 peak position at 398.20 eV[32,33]. Thus, the composite material possessed a somewhat different chemical environment than stand-alone g-C_3N_4 because of the $GdFeO_3$ and g-C_3N_4 interaction.

$GdFeO_3$ and g-C_3N_4 are capable of absorbing light up to 685 and 455 nm, respectively (see Fig. 4a). Thus, $GdFeO_3$ absorbs both visible and UV light. The $GdFeO_3$/g-C_3N_4 absorption intensity decreased as the g-C_3N_4 content increased. Additionally, the absorption edge of the $GdFeO_3$/g-C_3N_4 composites red-shifted relative to unmodified $GdFeO_3$ as the $GdFeO_3$ content in the sample increased. The wide light absorption range of the $GdFeO_3$/g-C_3N_4 composites was because of its bandgap decrease (relative to unmodified g-C_3N_4) from 2.83 to 2.22-2.02 eV (see Fig. 4b) [34].

The maximum of the UV–Vis absorption RhB under the presence of GFO/CN-3:7 was at 553 nm (see Fig. 5a). The peak intensity decreased with time, which confirms RhB decomposition under the GFO/CN-3:7 presence (also corroborated by the gradual RhB solution discoloration visible by the naked eye). A blue-shifted absorption peak was ascribed to the RhB deethylation[35]. Photodegradation efficiency of unmodified g-C_3N_4 and $GdFeO_3$ was low: only 9.5% and 41% of RhB was removed after 120 min of visible-light irradiation (see Fig. 5b). At the same time, GFO/CN-3:7 composite decomposed 92% of RhB (see Fig. 5b), which was the highest value among all other composites obtained in this work. The conclusion of experiment proves that exists an optimum composite ratio between $GdFeO_3$ and g-C_3N_4, which yields best efficiency[36].

We also performed photocatalytic reactions of RhB decomposition assisted by the GFO/CN-3:7 under the presence of radical- and hole-capturing compounds to understand which active oxygen species (AOSs) were dominant (see Fig. 6a). For this purpose, we added isopropyl alcohol (IPA) and p-benzoquinone (BQ) to quench hydroxyl (•OH) and superoxide ($\bullet O_2^-$) radicals, respectively[37]. Only 5.5% and almost 0% of RhB was removed after 120 min under the IPA and BQ presence (see Fig. 6). Thus, the main AOSs were •OH and $\bullet O_2^-$. We also added disodium ethylenediaminetetraacetate (EDTA-2Na) to quench holes and observed the decomposition of only 25.7% of RhB[37]. which means that the dye molecules can also be oxidated directly by the photogenerated holes occurs from separation of photoproduction electron-hole pairs.

spectra of $GdFeO_3$ showed almost no emission, while g-C_3N_4 showed strong fluorescence (see Fig. 7(a)). PL intensity of the GFO/CN composites was lower than that of g-C_3N_4. Thus, the electron-hole pair separation was because of g-C_3N_4 coupling with $GdFeO_3$. Out of all composites, GFO/CN-3:7 demonstrated the lowest PL emission intensity, which is indicative of the highest charge transfer efficiency and the possibility of the highest photocatalytic oxidation activity[38].

Fig. 7(b) shows EIS data obtained for g-C_3N_4, $GdFeO_3$, and GFO/CN-3:7. The radii of the semicircles are proportional to the charge transfer resistance. GFO/CN-3:7 exhibited the smallest semicircle, which is indicative of the best charge transfer efficiency and conductivity out of these three samples, which agrees with the PL data[39,40].

To be feasible for practical applications, a catalyst must be stable and reusable. To demonstrate this, we used GFO/CN-3:7 composite for three consecutive photocatalytic RhB degradation reactions performed

under the same conditions (see Fig. 8). During the first, second and third reactions, GFO/CN-3:7 was able to assist in decomposition of 92, 91 and 87% of the initial RhB. A slight decline of the RhB removal rate by the GFO/CN-3:7 catalyst was attributed to not fully recovered active sites, and minor weight loss occurred during post-reaction rinsing.

To explain such excellent photocatalytic activity of the GFO/CN-3:7 nanocomposite, we first used the concept of the band-edge potential levels and heterojunctions, which determines the separation and recombination of photoelectron-hole pairs. $GdFeO_3$ valence and conduction band (VB and CB, respectively) potentials were lower than those of g-C_3N_4. Thus, the electrons can travel from the g-C_3N_4 CB to the $GdFeO_3$ CB. Simultaneously, the photogenerated holes can move from the $GdFeO_3$ VB to the g-C_3N_4 VB. However, the E_{CB} of $GdFeO_3$ is above the $O_2/{\bullet}O_2^-$ potential (which is equal to -0.33 eV vs. NHE). Therefore, the hole transport from the $GdFeO_3$ VB is very slow, which lowers that material's photocatalytic activity.

Therefore, we considered a Z-scheme mechanism instead. The photogenerated electrons on the $GdFeO_3$ CB transfer with ease to the g-C_3N_4 VB, reacting with the g-C_3N_4 holes and inhibiting their recombination in both $GdFeO_3$ and g-C_3N_4. This, in turn, prolongs the time electrons and holes remain on the g-C_3N_4 CB and $GdFeO_3$ VB, respectively. These processes enhance the charge transfer at the g-C_3N_4/$GdFeO_3$ interface (see Fig. 9). At the same time, the electrons from g-C_3N_4 CB with strong reduction potential (equal to -1.14 eV react with O_2 producing ${\bullet}O_2^-$ (see Eq. (1)).

Yet, the holes on the $GdFeO_3$ VB could not oxidize •OH or H_2O to •OH since the $GdFeO_3$ VB potential is below that of •OH /OH^- (which is equal to 2.4 eV vs. NHE) [41,42]. The $GdFeO_3$ VB potential is above the redox potential of OH^-/•OH (equal to 1.99 eV vs. NHE). Thus, OH^- can be oxidized by holes to •OH (see Eq. (5)). Similar hole behavior was observed when a $CoFe_2O_4$ catalyst was used[43,44]. The g-C_3N_4 CB edge potential is below that of O_2/H_2O_2 (which is equal to 0.685 eV vs. NHE) [45]. Thus, •OH can form as a result of the reaction between the adsorbed oxygen and the photogenerated electrons: $O_2+2e^-+2H^+ = H_2O_2$, $H_2O_2 + e^- = {\bullet}OH + OH^-$.

Thus, the AOSs of the RhB degradation assisted by the g-C_3N_4/$GdFeO_3$ composite catalyst were ${\bullet}O_2^-$, •OH, and h^+. The separation of the electrons and holes very likely followed a Z-scheme charge transfer. The corresponding reactions can be described as shown below

$$GdFeO_3/g\text{-}C_3N_4 + h\nu \rightarrow GdFeO_3\,(e_{CB}^- + h_{VB}^+) + g\text{-}C_3N_4\,(e_{CB}^- + h_{VB}^+) \quad (1)$$

$$g\text{-}C_3N_4\,(e_{CB}^-) + O_2 \rightarrow {\bullet}O_2^- \quad (2)$$

$$g\text{-}C_3N_4\,(2e_{CB}^-) + O_2 + 2H^+ \rightarrow H_2O_2 \quad (3)$$

$$g\text{-}C_3N_4\,(e_{CB}^-) + H_2O_2 + {\bullet}O_2^- \rightarrow OH^- + {\bullet}OH \quad (4)$$

$GdFeO_3$ (h_{VB}^+)+OH^-→•OH (5)

•O_2^-+•OH+$GdFeO_3$ (h_{VB}^+)+RhB→Degradation products (CO_2+H_2O) (6)

4. Conclusions

This work reported the preparation of $GdFeO_3$/g-C_3N_4 catalyst with various $GdFeO_3$:g-C_3N_4 ratios. We used a simple ultrasonication-assisted synthesis approach. The resulting hybrid nanocomposites were tested for their photocatalytic activity towards RhB decomposition. GFO/CN-3:7 showed photocatalytic activity significantly higher than other composites and than unmodified $GdFeO_3$ and g-C_3N_4: 92% of RhB decomposed when the solution was exposed to the visible light for 120 mins. The photocatalytic mechanism was described as a Z-scheme with the •O_2^-, •OH, and h^+ being the most active species. EIS and PL data showed that such excellent activity was because of the very efficient separation of the photogenerated electron-hole pairs, which was accelerated by the interfacial charge carrier recombination. The results obtained in this work provide novel ideas on the development of very efficient visible-light photocatalysts and the usage of $GdFeO_3$/g-C_3N_4 composites for organic pollutant removal.

Declarations

Acknowledgments

We gratefully acknowledge the financial supports from the National Natural Science Foundation of China (22078121), the key Natural Science Foundation of Anhui Province (KJ2018A0463, KJ2018A0465), the key Science Foundation of Huainan Normal University (2018xj15zd), and the Natural Science Foundation of Anhui Province (1808085ME109).

References

[1] L. Zou, H. R. Wang, C. Wu et al., Construction of all-solid-state Z-scheme 2D $BiVO_4$/Ag/CdS composites with robust photoactivity and stability. Appl. Surf. Sci. **498,** 143900 (2019)

[2] A. M. Abu-Dief, A. A. Essawy, A. K. Diab et al., Facile synthesis and characterization of novel Gd_2O_3-CdO binary mixed oxide nanocomposites of highly photocatalytic activity for wastewater remediation under solar illumination. J. Phys. Chem. Solids. **148,** 109666 (2021)

[3] E. S. Baeissa, Environmental remediation of aqueous methyl orange dye solution via photocatalytic oxidation using Ag-$GdFeO_3$ nanoparticles. J. Alloy Compd. **678,** 267-272 (2016)

[4] J. R. Wu, W. W. Wang, Y. Tian et al., Piezotronic effect boosted photocatalytic performance of heterostructured $BaTiO_3$/TiO_2 nanofibers for degradation of organic pollutants. Nano Energy. **77,** 105122 (2020)

[5] Q. C. Zhang, L. Jiang, J. Wang et al., Photocatalytic degradation of tetracycline antibiotics using three-dimensional network structure perylene diimide supramolecular organic photocatalyst under visible-light irradiation. Appl. Catal. B Environ. **277,** 119122 (2020)

[6] N. T. D. Cam, H. D. Pham, T. D. Pham et al., Novel photocatalytic performance of magnetically recoverable $MnFe_2O_4/BiVO_4$ for polluted antibiotics degradation. Ceram. Int. **47,** 1686-1692 (2021)

[7] D. F. Xu, B. Cheng, S. W. Cao et al., Enhanced photocatalytic activity and stability of Z-scheme Ag_2CrO_4-GO composite photocatalysts for organic pollutant degradation. Appl. Catal. B Environ. **164,** 380-388 (2015)

[8] Y. Gong, X. Quan, H. T. Yu et al., Synthesis of Z-scheme $Ag_2CrO_4/Ag/g\text{-}C_3N_4$ composite with enhanced visible-light photocatalytic activity for 2,4-dichlorophenol degradation. Appl. Catal. B Environ. **219,** 439-449 (2017)

[9] H. T. Li, N. Li, M. Wang et al., Synthesis of novel and stable $g\text{-}C_3N_4\text{-}Bi_2WO_6$ hybrid nanocomposites and their enhanced photocatalytic activity under visible light irradiation. Roy. Soc. Open Sci. **5,** 171419 (2018)

[10] T. F. Yu, C. W. Chang, P. W. Chung et al., Unsupported and silica- supported perovskite-type lanthanum manganite and lanthanum ferrite in the conversion of ethanol. Fuel Process. Technol. **194,** 106117 (2019)

[11] M. A. Gabal, F. Al-Solami, Y. M. A. Angari et al., Auto-combustion synthesis and characterization of perovskite- type $LaFeO_3$ nanocrystals prepared via different routes. Ceram. Int. **45,** 16530-16539 (2019)

[12] A. A. Hoseini, S. Farhadi, A. Zabardasti et al., A novel n-type CdS nanorods/p-type $LaFeO_3$ heterojunction nanocomposite with enhanced visible-light photocatalytic performance. RSC Adv. **9,** 24489-24504 (2019)

[13] Y. L. Niea, L. L. Zhang, Y. Y. Li et al., Enhanced Fenton-like degradation of refractory organic compounds by surface complex formation of $LaFeO_3$ and H_2O_2. J. Hazard Mater. **294,** 195-200 (2015)

[14] C. X. Qin, Z. Y. Li, G. Q. Chen et al., Fabrication and visible-light photocatalytic behavior of perovskite praseodymium ferrite porous nanotubes. J. Power Sources **285,** 178-184 (2015)

[15] M. S. Zhu, C. Y. Zhai, M. J. Sun et al., Ultrathin graphitic C_3N_4 nanosheet as a promising visible-light-activated support for boosting photoelectrocatalytic methanol oxidation. Appl.Catal. B Environ. **203,** 108-115 (2017)

[16] Y. P. Che, B. X. Lu, Q. Qi et al., Bio-inspired Z-scheme $g\text{-}C_3N_4/Ag_2CrO_4$ for efficient visible-light photocatalytic hydrogen generation. Sci Rep. **8,** 16504 (2018)

[17] J. N. Qu, Y. Du, Y. B. Feng et al., Visible-light-responsive K-doped $g\text{-}C_3N_4$/BiOBr hybrid photocatalyst with highly efficient degradation of Rhodamine B and tetracycline. Mater. Sci. Semicond. Process. **112,**

105023 (2020)

[18] J. Di, J. X. Xia, S. Yin et al., Preparation of sphere-like g-C_3N_4/BiOI photocatalysts via a reactable ionic liquid for visible- light-driven photocatalytic degradation of pollutants. J. Mater. Chem A. **2,** 5340-5351 (2014)

[19] T. Fan, C. C. Chen, Z. H. Tang et al., Synthesis and characterization of g-C_3N_4/$BiFeO_3$ composites with an enhanced visible light photocatalytic activity. Mat Sci. Semicon Proc. **40,** 439-445 (2015)

[20] L. Q. Zhang, X. He, X. W. Xu et al., Highly active TiO_2/g-C_3N_4 /G photocatalyst with extended spectral Response towards selective reduction of nitrobenzene. Appl. Catal. B Environ. **203,** 1-8 (2017)

[21] J. Ren, Y. Z. Wu, H. Zou et al., Synthesis of a novel $CeVO_4$/graphitic C_3N_4 composite with enhanced visible- light photocatalytic property. Mater. Lett. **183,** 219-222 (2016)

[22] M. Ismael, E. Elhaddad, D. H. Taffa et al., Solid state route for synthesis of $YFeO_3$/g-C_3N_4 composites and its visible light activity for degradation of organic pollutants. Catal. Today. S0920586118300543 (2018)

[23] L. Li, X. Wang, Y. Lan et al., Synthesis, photocatalytic and electrocatalytic activities of wormlike $GdFeO_3$ nanoparticles by a glycol- assisted sol-gel process. Ind. Eng. Chem. Res. **52,** 9130-9136 (2013)

[24] W. Yu, L. Zou, H. R. Wang et al., Novel $Bi_{12}TiO_{20}$/g-C_3N_4 composite with enhanced photocatalytic performance through Z-scheme mechanism. J. Mater. Sci. **53,** 10039-10048 (2018)

[25] J. Ren, Y. Z. Wu, Y. Dai et al., Enhanced visible-light-driven photocatalytic activity of $CeVO_4$ /graphitic C_3N_4 photocatalysts for organic dye degradation. Mater. Technol. **32,** 574-583(2017)

[26] Y. Wu, H. Wang, W. G. Tu et al., Quasi-polymeric construction of stable perovskite-type $LaFeO_3$/g-C_3N_4 heterostructured photocatalyst for improved Z-scheme photocatalytic activity via solid p-n heterojunction interfacial effect. J. Hazard. Mater. **347,** 412-422 (2018)

[27] Yan. L. Lia, N. F. Chen, J. P. Zhou et al., Effect of the oxygen concentration on the properties of Gd_2O_3 thin films. J. Cryst. Growth **265,** 548-552 (2004)

[28] J. A. Gupta, D. Landheer, J. P. McCaffrey et al., Gadolinium silicate gate dielectric films with sub-1.5 nm equivalent oxide thickness. Appl. Phys. Lett. **78,** 1718-1720 (2001)

[29] L. Q. Jing, H. G. Fu, B. Q. Wang et al., Effects of Sn dopant on the photoinduced charge property and photocatalytic activity of TiO_2 nanoparticles. Appl. Catal. B **62,** 282-291 (2006)

[30] J. C. Wang, H. C. Yao, Z. Y. Fan et al., Indirect Z-scheme BiOI/g-C_3N_4 photocatalysts with enhanced photoreduction CO_2 activity under visible light irradiation. ACS Appl. Mater. Interfaces. **8,** 3765-3775

(2016)

[31] J. J. Wang, L. Tang, G. M. Zeng et al., Plasmonic Bi metal deposition and g-C_3N_4 coating on Bi_2WO_6 microspheres for efficient visible-light photocatalysis. ACS Sustainable Chem. Eng. **5,** 1062-1072 (2017)

[32] H. F. Wang, Y. G. Xu, L. Q. Jing et al., Novel magnetic $BaFe_{12}O_{19}$/g-C_3N_4 composites with enhanced thermocatalytic and photo-Fenton activity under visible-light. J. Alloys Compd **710,** 510-518 (2017)

[33] Y. G. Xu, H. Xu, J. Yan et al., A plasmonic photocatalyst of Ag/AgBr nanoparticles coupled withg-C_3N_4 with enhanced visible-light photocatalytic ability. Colloids Surf., A: Physicochem. Eng. Aspects **436,** 474-483 (2013)

[34] J. Luo, X. S. Zhou, L. Ma et al., Rational construction of Z-scheme Ag_2CrO_4/g-C_3N_4 composites with enhanced visible-light photocatalytic activity. Appl. Surf. Sci. **390,** 357-367 (2016)

[35] X. W. Li, J. X. Xia, W. S. Zhu et al., Facile synthesis of few-layered MoS_2 modified BiOI with enhanced visible-light photocatalytic activity. Colloids Surf., A Physicochem. Eng. Aspects **511,** 1-7 (2016)

[36] H. R. Wang, L. Zou, Y. C. Shan et al., Ternary GO/Ag_3PO_4/AgBr composite as an efficient visible-light-driven photocatalyst. Mater. Res. Bull. **97,** 189-194 (2018)

[37] F. Guo, W. L. Shi, H. B. Wang et al., Study on highly enhanced photocatalytic tetracycline degradation of type II AgI/$CuBi_2O_4$ and Z-scheme AgBr/$CuBi_2O_4$ heterojunction photocatalysts. J. Hazard. Mater. **349,** 111-118 (2018)

[38] L. Z. Liu, T. P. Hu, K. Dai et al., A novel step-scheme $BiVO_4$/Ag_3VO_4 photocatalyst for enhanced photocatalytic degradation activity under visible light irradiation. Chin. J. Catal. **42,** 46-55 (2021)

[39] S. L. Prabavathi, K. Saravanakumar, C. M. Park et al., Photocatalytic degradation of levofloxacin by a novel Sm_6WO_{12}/g-C_3N_4 heterojunction: Performance, mechanism and degradation pathways. Sep. Purif. Technol. **257,** 117985 (2021)

[40] K. Saravanakumar, V. Muthuraj, S. Vadivel, Constructing novel Ag nanoparticles anchored on MnO_2 nanowires as an efficient visible light driven photocatalyst. RSC Adv. **6,** 61357-61366 (2016)

[41] X. J. Wen, C. G. Niu, H. Guo et al., Photocatalytic degradation of levofloxacin by ternary Ag_2CO_3/CeO_2/AgBr photocatalyst under visible-light irradiation: degradation pathways, mineralization ability, and an accelerated interfacial charge transfer process study. J. Catal. **358,** 211-223 (2018)

[42] X. J. Wen, Q. Lu, X. X. Lv et al., Photocatalytic degradation of sulfamethazine using a direct Z-Scheme AgI/$Bi_4V_2O_{11}$ photocatalyst: Mineralization activity, degradation pathways and promoted charge separation mechanism. J. Hazard. Mater. **385,** 121508 (2020)

[43] L. Gan, S. M. Shang, C. W. M. Yuen et al., Hydrothermal synthesis of magnetic $CoFe_2O_4$/Graphene nanocomposites with improved photocatalytic activity. Appl. Surf. Sci. **351,** 140-147 (2015)

[44] L. Q. Jing, Y. G. Xu, S. Q. Huang et al., Novel magnetic $CoFe_2O_4$/Ag/Ag_3VO_4 composites:Highly efficient visible light photocatalytic and antibacterial activity. Appl. Catal. B Environ. **199,** 11-22 (2016)

[45] Q. Liu, T. X. Chen, Y. R. Guo et al., Grafting Fe(III) species on carbon nanodots/Fe-doped g-C_3N_4 via interfacial charge transfer effect for highly improved photocatalytic performance. Appl. Catal. B Environ. **205,** 173-181 (2017)

Figures

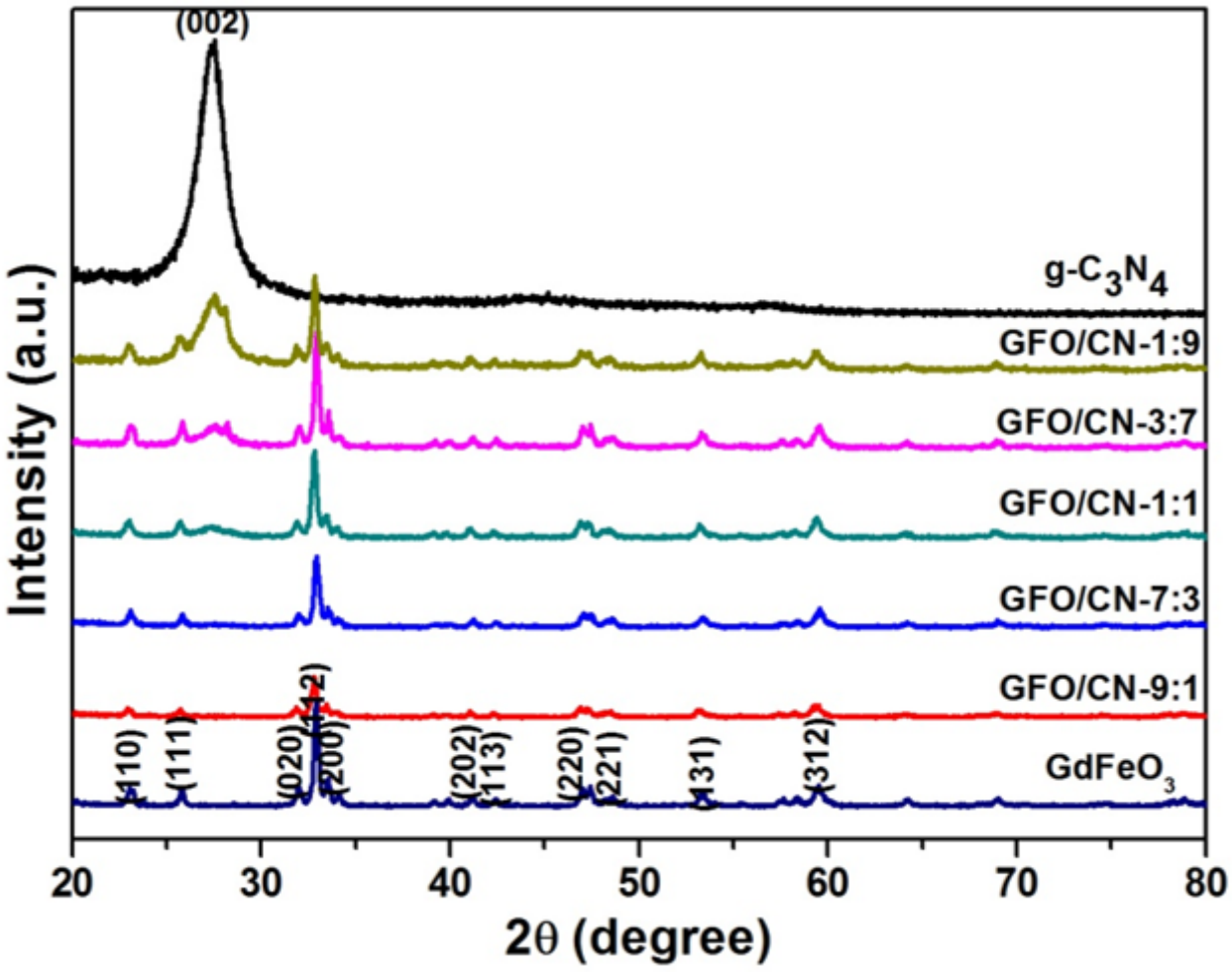

Figure 1

XRD pattern of GdFeO3, g-C3N4 and GdFeO3/g-C3N4 composites.

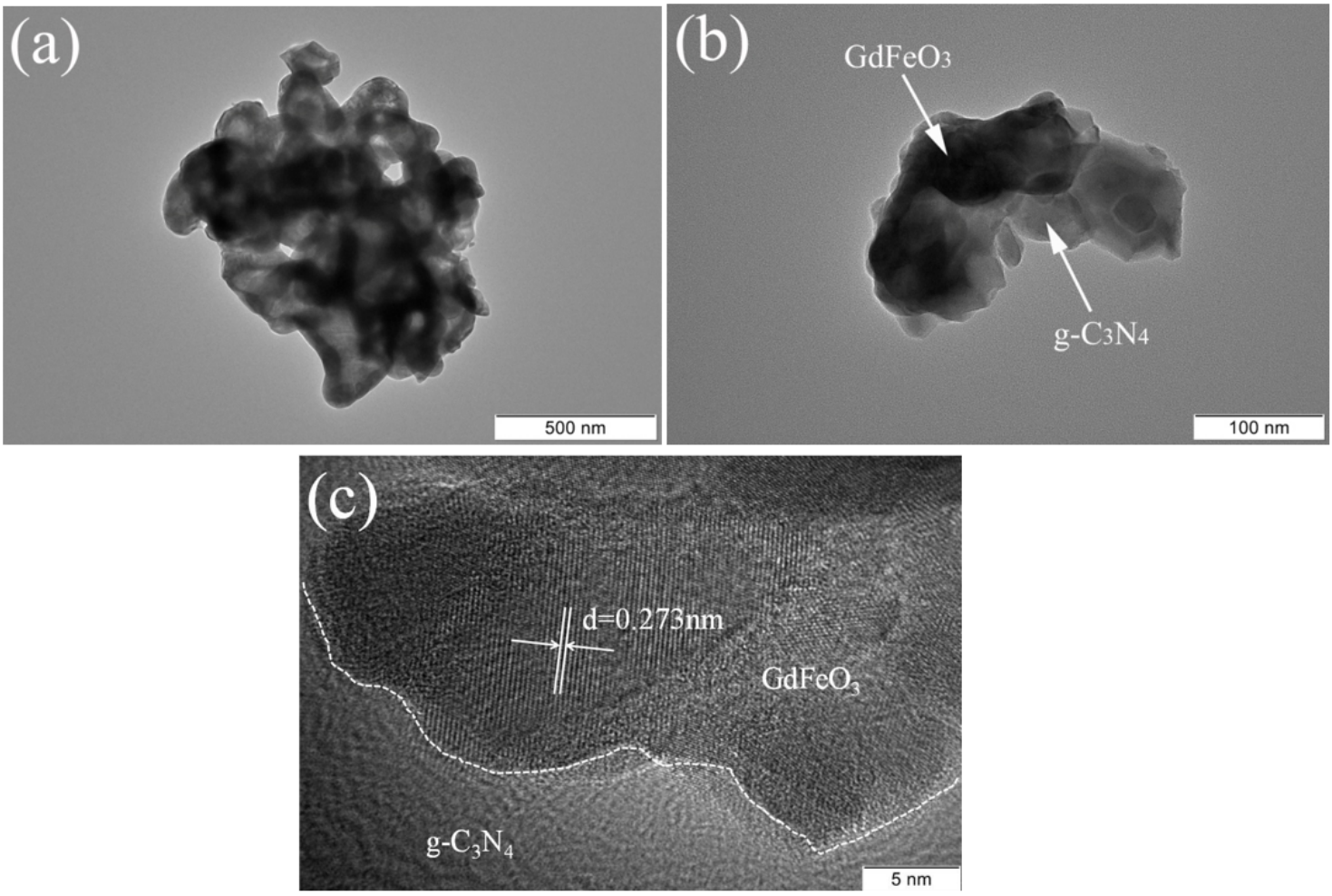

Figure 2

The TEM (a), (b) and (c) HRTEM pattern of GFO/CN-3:7.

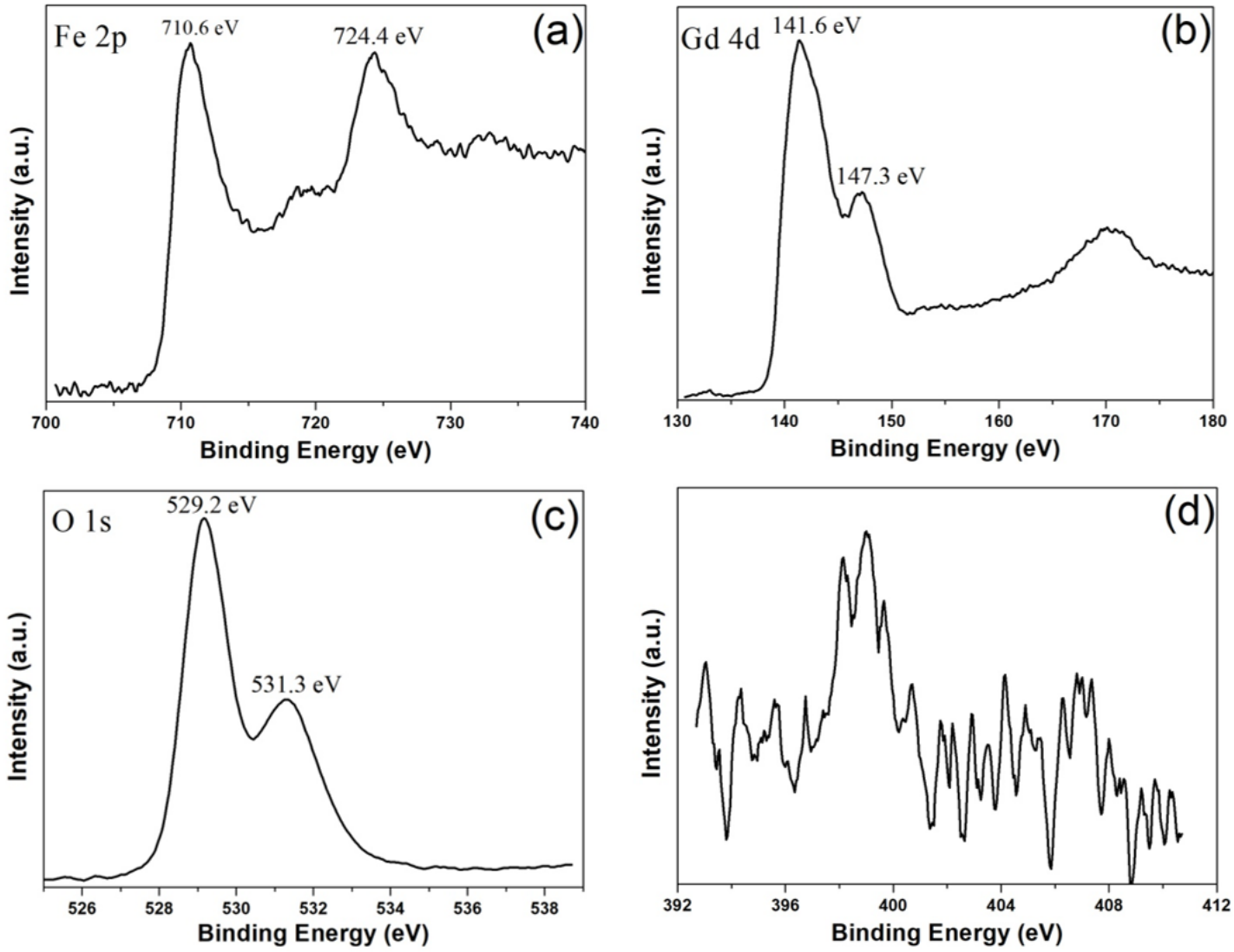

Figure 3

XPS survey spectrum of (a)Fe 2p, (b) Gd 4d, (c) O 1s, and (d) N 1s of GFO/ CN-3:7 sample.

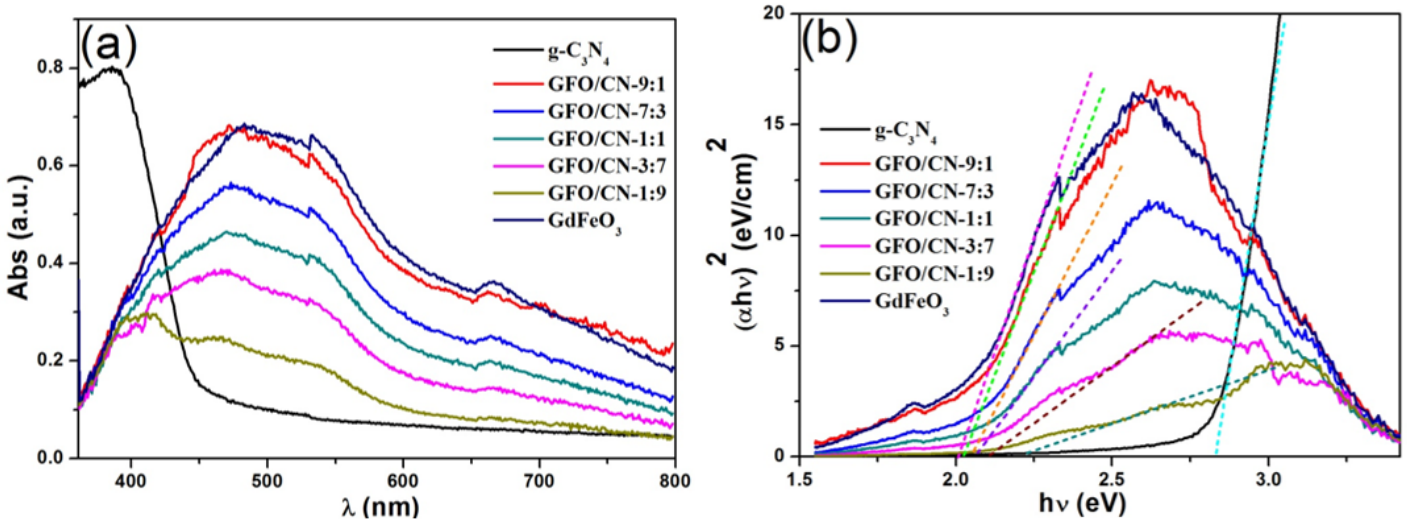

Figure 4

UV–vis diffuse reflectance spectra (a), the estimated band gap (b) of the GdFeO3, g-C3N4 and GdFeO3/g-C3N4 composites

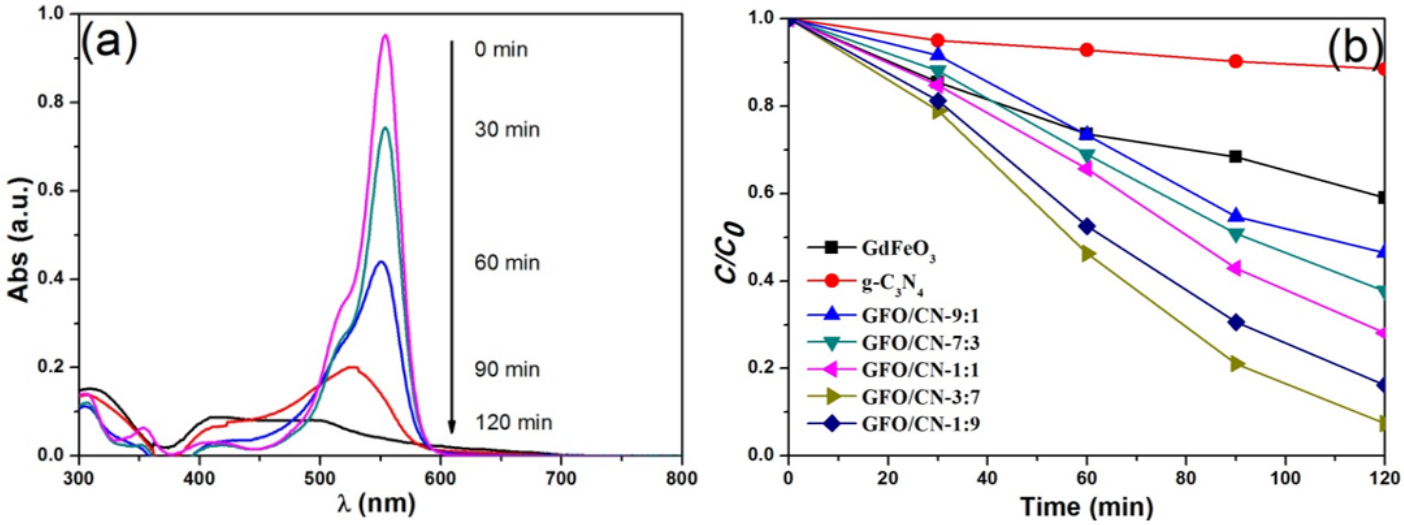

Figure 5

(a) Changes in UV-Vis absorption spectra of RhB in the presence of GFO/ CN=3:7 composite with irradiation time, (b) Photodegradation efficiencies of RhB as a function of irradiation time at different photocatalysts.

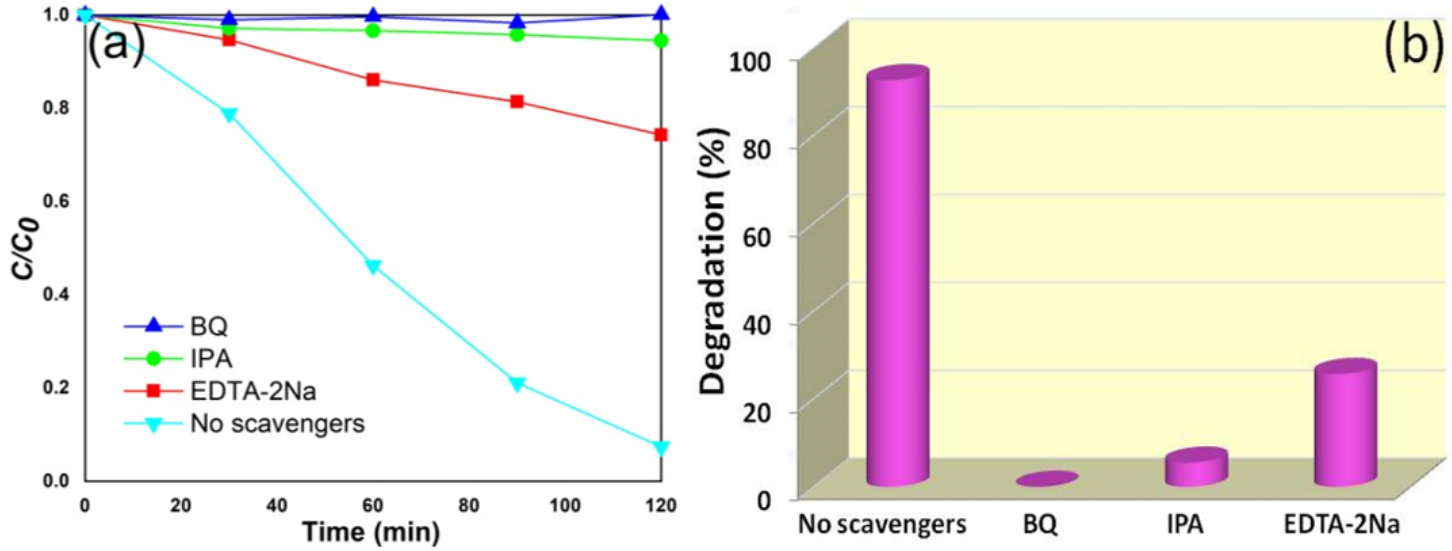

Figure 6

(a) Photodegradation and (b) visible light photodegradation of RhB over GFO/ CN=3:7 sample in the presence of different scavengers during 120 min.

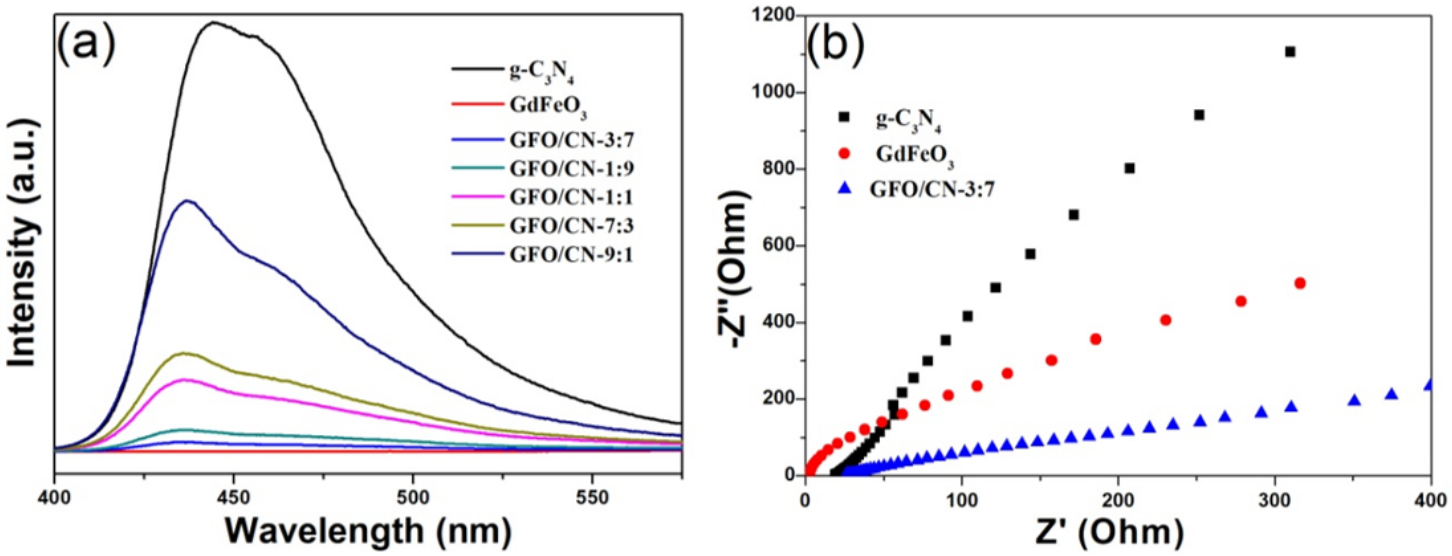

Figure 7

(a) Room-temperature PL spectra of all as-prepared samples (λEx = 300 nm); (b) EIS Nyquist plots of GdFeO3, g-C3N4 and GFO/CN-3:7.

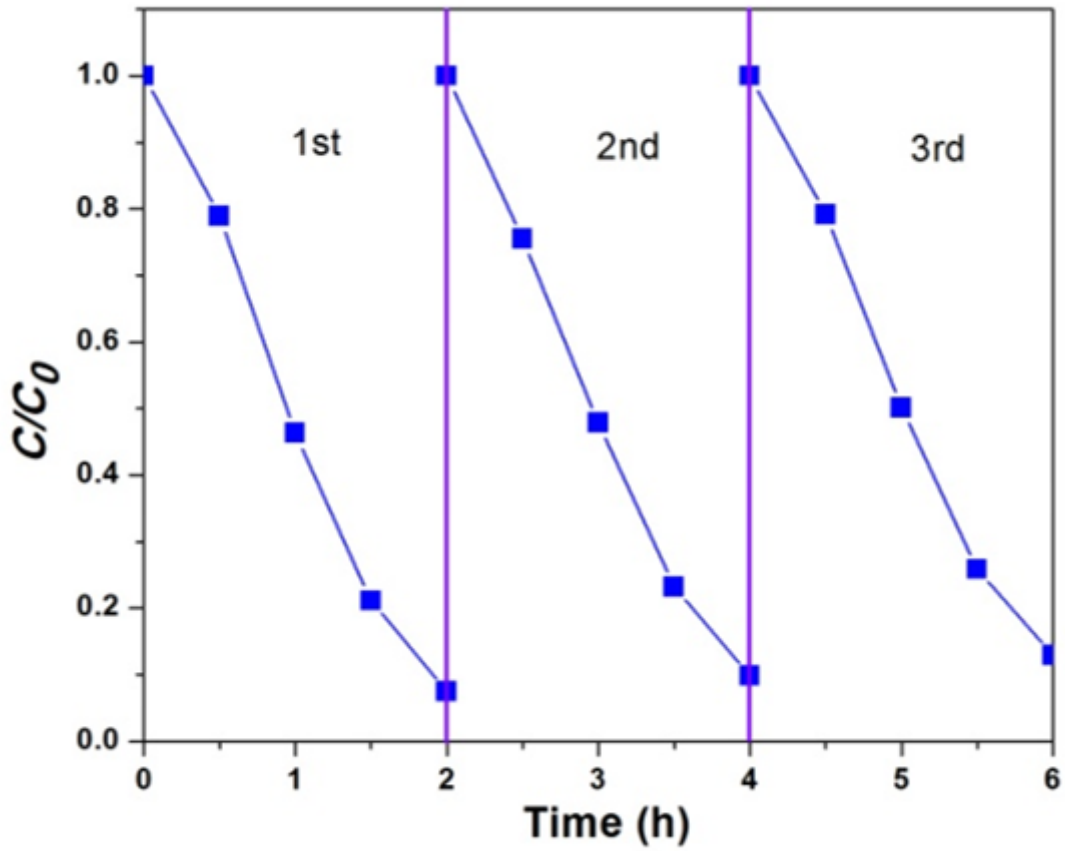

Figure 8

Recycling test of the GFO/CN-3:7 composite with each run lasting for 2 h under visible light irradiation.

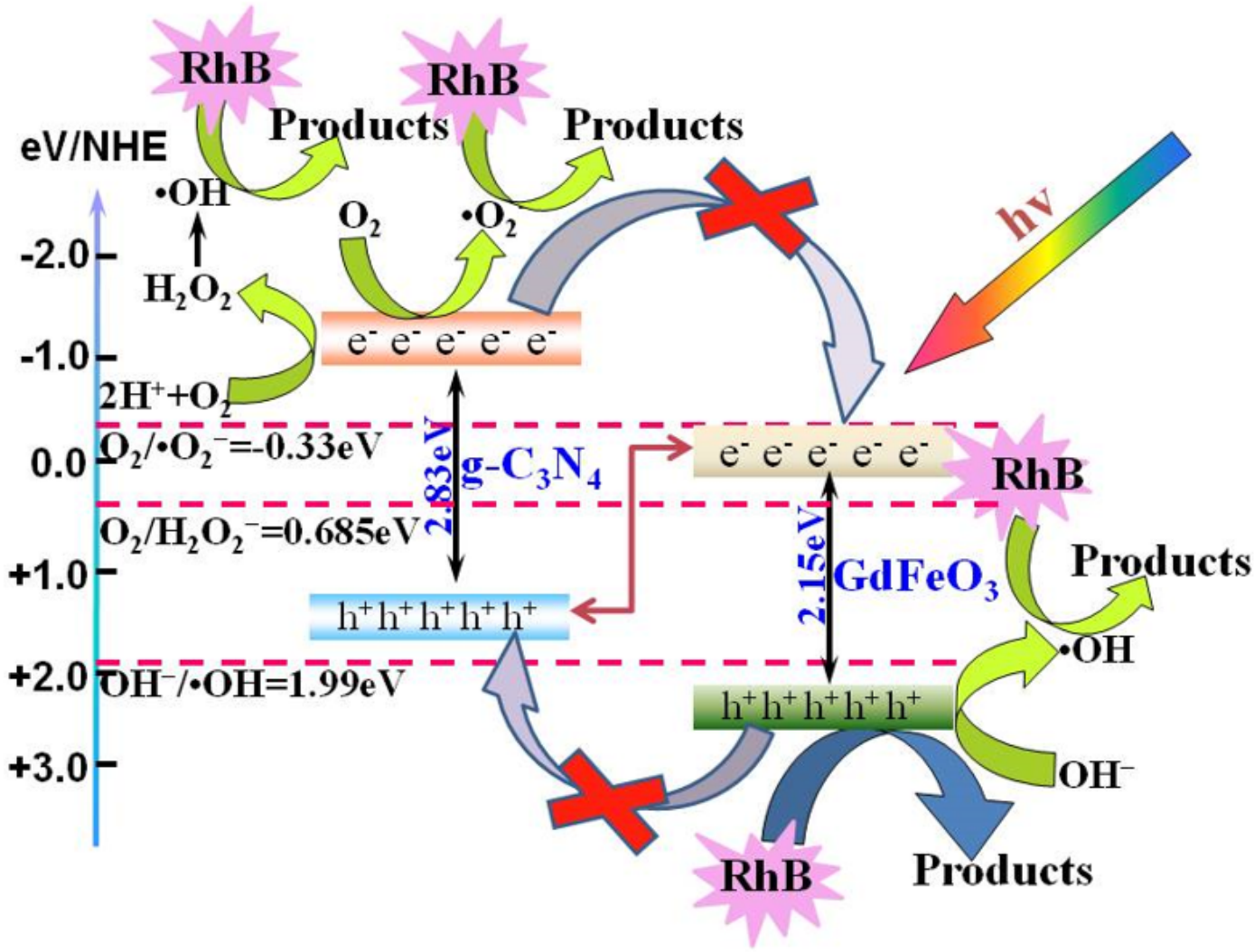

Figure 9

Schematic illustration for the electron/hole pairs separation and transport processes and visible-light-driven photocatalysis in the GFO/CN-3:7 composite.